https://doi.org/10.5194/egusphere-2025-2647
Preprint. Discussion started: 23 June 2025

Morphological and topographic profile analysis of shallow landslides inside and outside of forests with a semi-automatic mapping approach and bi-temporal airborne laser scanning data

Lotte de Vugt[1], Thomas Zieher[2], Barbara Schneider-Muntau[3], Frank Perzl[2], Marc Adams[2] and Martin Rutzinger[1]

[1]Department of Geography, University of Innsbruck, Innsbruck, 6020, Austria
[2]Austrian Research Centre for Forests, Innsbruck, 6020, Austria
[3]Unit of Geotechnical Engineering, University of Innsbruck, Innsbruck, 6020, Austria

Correspondence to: Lotte de Vugt (Lotte.De-Vugt@student.uibk.ac.at)

Abstract. Investigating the effects of forest land cover on shallow landslide characteristics such as their morphology (e.g., area and mean depth) and topographic profiles could provide a better understanding of how forest affect landslide processes. Landslides located under the forest canopy, which are often overlooked by conventional landslide mapping methods (e.g., using aerial imagery), can be captured using airborne laser scanning (ALS). In this study we investigated forest effects on landslides by developing a well-performing semi-automated workflow for mapping landslide scars and analysing their characteristics in relation to the forest canopy cover, using terrain models from ALS data. The mapped landslide scars were analysed with a forest canopy cover mask and forest structure parameters, such as the closest tree distance and the number of trees surrounding the scar. The investigated scars within the forest have significantly larger depths, thicknesses and higher pre-failure slope values than scars located outside the forests. Additionally, the differences are clearer when forest structure parameters are considered, of which the closest tree distance showed the strongest relation to the landslide characteristics. The evidence aids better understanding of how forests affect landslide processes and how they serve their protective function.

1 Introduction

Shallow landslides (regolith slides with a depth < 2 m below the surface) are a worldwide phenomenon that is well studied (Guzzetti, 2021). Within shallow landslide research there is still a large knowledge gap concerning the occurrence of shallow landslides in forested areas and specifically the effect of forest land cover on landslide processes. Forests are known to have a positive effect on slope stability (Cohen and Schwarz, 2017; Gonzalez-Ollauri and Mickovski, 2017; Schwarz et al., 2010). However, the exact effects of forest land cover on landslide processes is something that still needs to be researched in more detail (Greco et al., 2023). A first step in the direction of this understanding would be the analysis of the differences between the characteristics of shallow landslides occurring in forests (areas with high tree density) and those occurring outside of forests (areas with low to zero tree density, such as grasslands). Landslide characteristics, such as their topographic profile and morphology (e.g., their area and mean depth characteristics), can tell us something about the processes behind the occurrence

https://doi.org/10.5194/egusphere-2025-2647
Preprint. Discussion started: 23 June 2025

of these landslides (Taylor et al., 2018). In addition, these characteristics support quantifications of landslide magnitude and their potential impacts on their environment (Koyanagi et al., 2020; Rickli and Graf, 2009).

Many studies have already investigated the morphology of shallow landslides (Malamud et al., 2004; Taylor et al., 2018; Zieher et al., 2016) and in some cases also more detailed topographic characteristics (Emberson et al., 2022). However, only a few have focussed specifically on forested areas (Görüm, 2019; Koyanagi et al., 2020; Razak et al., 2011; Rickli and Graf, 2009; Schmaltz et al., 2017). Some of the few studies that investigated the differences between landslides inside and outside forests showed that there may be differences between landslides within and outside the forest (Koyanagi et al., 2020; Rickli and Graf, 2009). However, it should be noted that Rickli and Graf (2009) did not find consistent results across the investigated areas. A major reason for the lack of research investigating landslides in forests is related to the limited availability of inventories explicitly including landslides under forest canopies. Most studies investigating landslide characteristics use landslide inventories based on aerial or satellite imagery mapping, sometimes in combination with mapping from field work (Guzzetti et al., 2012). However, it is proven that the limitations of these methods create inventories biased against landslides under dense canopy cover (Schmaltz et al., 2017). Especially smaller landslides are easily missed or completely obscured under forest canopies (Brardinoni and Church, 2004).

It is becoming more common to use airborne laser scanning (ALS) in the preparation of landslide inventories (Ardizzone et al., 2007; Petschko et al., 2016; Schmaltz et al., 2017; Zieher et al., 2016). Topographic laser scanning has the capability of capturing terrain topography under dense vegetation cover (Wehr and Lohr, 1999) and use of such datasets in landslide inventory preparation can overcome the bias of conventional methods against landslides within forests. However, only the study by Schmaltz et al. (2017), which investigates the occurrence of landslides in relation to different forest cover types, was found to have also used ALS data in the extraction of landslide characteristics, such as pre-failure slope values. Although the study by Schmaltz et al. (2017) give an insight into how different silvicultural practices affect the probability of landslide occurrence in forest, their influence on landslide characteristics was not investigated.

Another issue with existing studies is the large variety in the methods used for deriving landslide characteristics, resulting in a lack of comparability between the results from different studies (Ardizzone et al., 2007; Galli et al., 2008; Guzzetti et al., 2012; Mondini et al., 2014). Most studies rely heavily on expert-based decisions in the delineation of the landslides due to a limited degree of automation in most methods. In addition, the delineation of landslides and the extraction of their characteristics is also highly dependent on the used source, which also results in large discrepancies between different studies (Galli et al., 2008). For example, some studies report landslide characteristics derived from aerial or satellite imagery (Fiorucci et al., 2011; Mondini et al., 2014), others report field measurements (Cardinali et al., 2006; Rickli and Graf, 2009), data derived from topographic laser scanning elevation models (Zieher et al., 2016) or in some cases combinations of the above (Ardizzone et al., 2007; Koyanagi et al., 2020; Schmaltz et al., 2017). Thus, there is also a need for using transparent and favourably transferable workflows when mapping and describing shallow landslides.

The main aim of this study is to analyse and compare the characteristics of shallow landslides scars (i.e., the depletion zone) within and outside of forests, which were triggered in an Alpine valley during an extreme rainfall event in June 2015. A

https://doi.org/10.5194/egusphere-2025-2647
Preprint. Discussion started: 23 June 2025

secondary objective of the study is to delineate and extract the characteristics of the shallow landslides with a semi-automated mapping approach based on multi-temporal digital terrain models (DTMs) from ALS data. Specifically, the study investigates how landslides inside forests and outside forests are represented in the pre-event DTM and the difference of DTMs (DoD) from the pre-and post-event data. To achieve method transferability and transparency, the analysis is performed on an inventory that is constructed using a semi-automatic approach. Since the characteristics are derived automatically from remote sensing data, the method transferability and transparency also apply to the extraction of the landslide characteristics. Based on our data and analyses the following research questions were investigated:

- Which differences can we see in the distributions of morphological and topographic profile characteristics of landslides inside and outside of forests, considering pre-event DTM and DoD data?
- Are these differences also related to differences in forest structure, such as proxies for tree density?
- Can these differences be explained from the differences in the processes behind these landslides?

2 Study Area

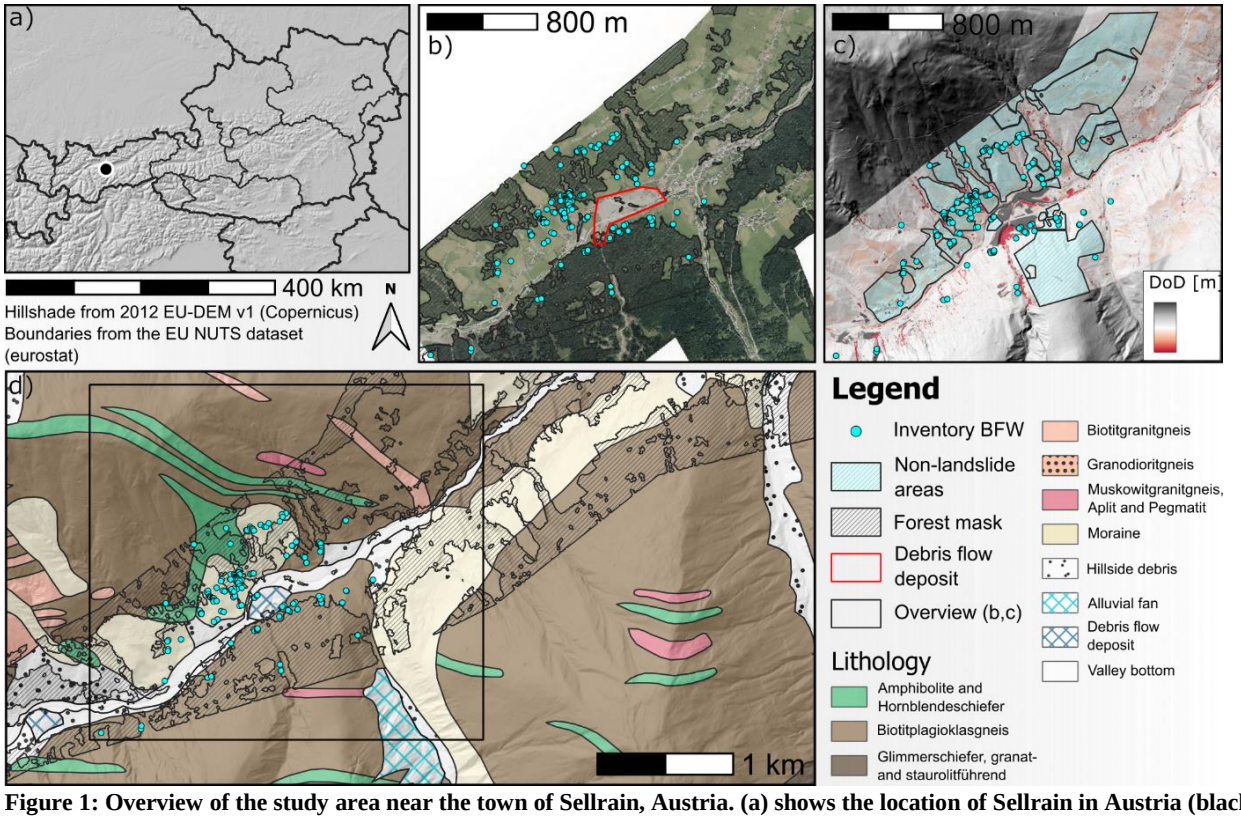

Figure 1: Overview of the study area near the town of Sellrain, Austria. (a) shows the location of Sellrain in Austria (black dot); (b) the focus area of the training datasets with the post-event orthophoto (provided by the federal state of Tyrol), the BFW inventory, the forest mask and location of the debris flow deposit; (c) shows the same focus area with the 2017 ALS DTM hillshade and 2017-2013 DoD (data provided by the federal state of Tyrol), the non-landslide areas and the BFW inventory (d) the full study area with the lithological map (GeoSphere Austria, 2021), the 2017 ALS DTM hillshade, the forest mask and BFW inventory.

https://doi.org/10.5194/egusphere-2025-2647
Preprint. Discussion started: 23 June 2025

2.1 The Sellrain valley

To investigate the differences between landslides within and outside the forest, the study focusses on the occurrence of a large number of shallow landslides within the Sellrain Valley, Tyrol (Austria) that were triggered by a severe rainfall event. This event is highly suited for this investigation as the event included both landslides within and outside the forests, according to an official landslide inventory from the Austrian Research Centre for Forests (BFW) (Figure 1). In addition to the considerable number of shallow landslides, the rainfall event also triggered a large debris flood in the Seigesbach torrent. The depositional area of the debris flood near the village of Sellrain is highlighted in Figure 1b. Although the debris flood area is not excluded from the investigations in this study, the topography and process behind the debris flood, as well as the related channel bank failures and bed erosion, are not further investigated. A more detailed description of this debris flow event is given in Adams et al. (2016).

The investigated area focused on an area of 8 km^2, limited by the coverage of the DoD, around the village Sellrain. The DoD covers the lower elevation sections of the valley with elevations ranging between 780 and 1410 m.a.s.l.. The valley is incised by the Melach river flowing from southeast to northwest. The study area also includes a section of the Seigesbach catchment (stretching in south-southeast to north-northwest direction) which terminates in the Melach river just west of the town Sellrain. The village Sellrain is located on the alluvial fan of this torrent. The study area is further characterised by steep slopes with an average slope angle of 28°. With regards to the geology, the study area is part of the Ötztal-Stubai crystalline complex, with formations mainly consisting of gneisses (e.g., “Schiefergneis”) and side moraine deposits (Moser, 2011) (Figure 1d). An analysis of the forest canopy cover mask created in this study shows that 46% of the study area is covered by forest (a high tree density), with the remaining landcover consisting of grassland (used mainly as meadows) and built-up areas. The predominant forest ecosystem is montane silicate spruce forest, consisting mainly of Norway spruce (Picea abies) with an admixture of European larch (Larix decidua) and of single trees or patches of grey alder (Alnus incana) and birch (Betula pendula) (Land Tirol, 2014). In addition, an analysis with the forest mask also showed that the slopes are generally steeper within the forest with an average slope angle of 33° against an average of 23° outside the forest mask.

2.1 Rainfall event characteristics

The investigated event occurred 7-8 June 2015. In the night of the 7th, 100-150 mm rain fell within a span of 12 hours (Lagger, 2015). According to a reanalysis of weather radar data (GeoSphere Austria, 2015), the event was very short and intense (Figure 2). Rainfall started at 19:00 UTC on the 7th with 7 mm h^{-1}. The peak occurred at 20:00 UTC with almost 60 mm h^{-1}. After 22:00 UTC the rainfall had already fallen below 5 mm h^{-1} and below 1 mm h^{-1} at 02:00. It should also be noted that May was wetter than average (Jenner, 2015) and it can thus be expected that the antecedent moisture content also played a role in the landslide occurrence.

https://doi.org/10.5194/egusphere-2025-2647
Preprint. Discussion started: 23 June 2025

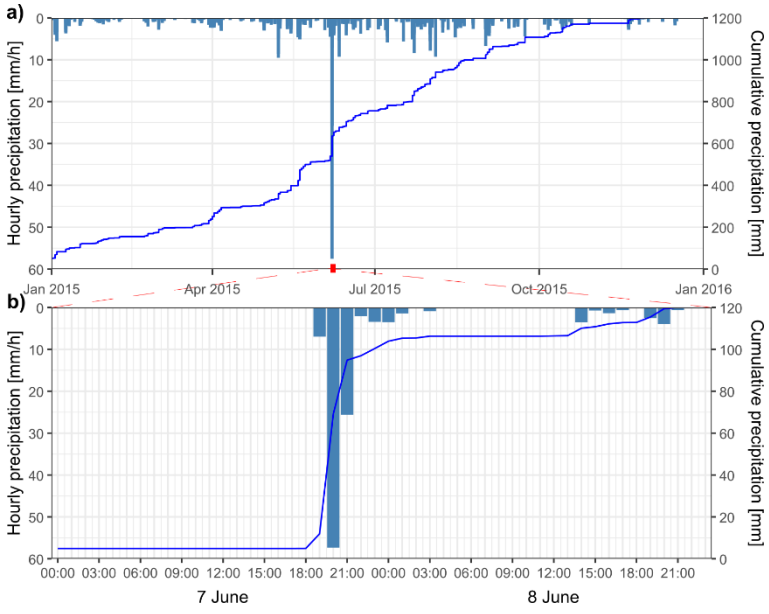

Figure 2: Reanalysis of the rainfall event with radar data from the INCA dataset (GeoSphere Austria, 2015). (a) Hourly precipitation data for the entire year 2015. (b) Hourly precipitation data for 7 and 8 June 2015.

2.1 Landslide mapping in the field

The landslide inventory that was constructed by the BFW found 136 landslides related to the event (Figure 1). This inventory includes a point-based dataset collected in the field and from visual inspection of an orthophoto taken on the 10 June 2015 (Figure 1b). The area of interest for the inventory was the area around the town of Sellrain and the area along the Seigesbach. A first analysis of the inventory with a canopy cover mask (Section 3.2; Figure 1b and d) shows that only 10 landslides are located within the areas with high tree density. Therefore, an important step of this study was to first detect additional landslides within the forests, because the BFW inventory may systematically underestimate them.

3 Materials and methods

An overview of the full workflow is given in Figure 3. The first main step of the workflow consisted of collecting, pre-processing and creating all the datasets that would be used in further analyses of the landslides, including the construction of a forest canopy cover mask. Since the existing landslide inventory from the BFW is a point-based inventory, the second main step of the workflow was to develop a polygon-based inventory from the existing points using a seeded region growing algorithm. The second main step also consisted of delineating areas without landslide signs in the DoD and orthophoto data, further referred to as non-landslide areas. Both datasets were used for validation and training in later steps of the workflow. The third main step of the workflow was to detect additional landslides within the forest, since the BFW inventory only contained limited samples within that category. For this, a random forest (RF) model was trained on the polygon-based,

https://doi.org/10.5194/egusphere-2025-2647
Preprint. Discussion started: 23 June 2025

segmented BFW inventory and the non-landslide areas using DoD data derived from two ALS acquisitions before and after the 2015 event. After the model was trained, a filtering and segmentation algorithm was used on the probability output of the RF model to construct the landslide detection map. The fourth main step in the workflow consisted of mapping the scars (the depletion zone) within the detected landslide areas. The final main step in the workflow was then to analyse the morphological and topographic profile characteristics of the mapped scars and the relationship of these characteristics with the location of the scars relative to the forest canopy cover mask and surrounding trees. For this the scars were classified into located within the forests (in this study defined by a share of the canopy cover mask ≥ 90%) and located outside the forest (in this study defined by a share of the canopy cover mask = 0%). Additionally, the scars were also analysed based on the average closest tree distance from each scar cell and the average number of trees within a 10 m radius of the scar cells.

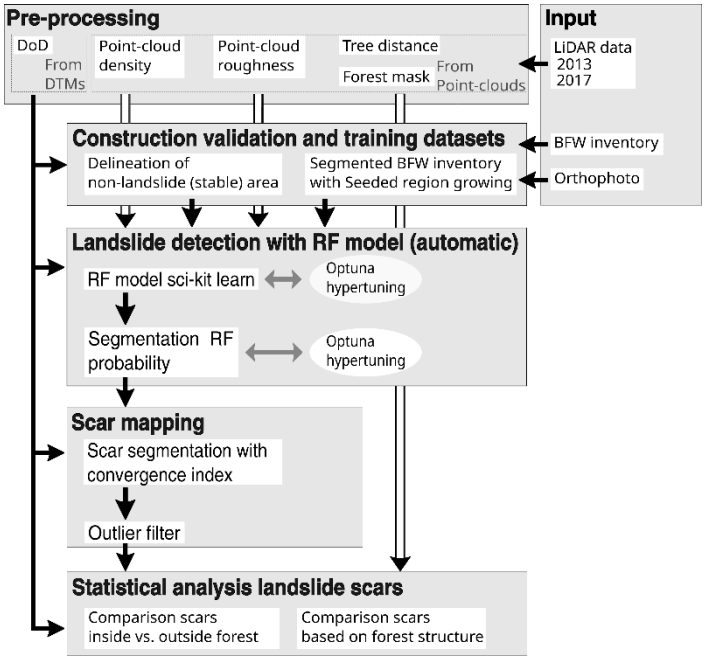

Figure 3: General workflow of the study.

3.1 Available datasets and pre-processing

Several datasets were used for the analysis of the landslide scars in the Sellrain valley, of which two ALS acquisitions from 2013 and 2017 were the most important. These datasets were provided by Federal State of Tyrol as classified point-cloud and their corresponding 0.5 m resolution DTMs.

The ALS datasets were used to construct a DoD from the provided DTMs. In addition to this, the 2013 ALS dataset was also used to construct a binary forest canopy cover mask. The LIS PRO grid-based forestry toolchain from SAGA LIS PRO v9.7.0 (Eysn et al., 2012) was used to extract single tree positions and a binary canopy cover map from a canopy height model constructed with the 2013 point-cloud data, using a tree height threshold at 2 m. The binary canopy cover mask was created by thresholding the canopy cover at 30%. The single tree positions were also used to construct a tree distance map and a tree

https://doi.org/10.5194/egusphere-2025-2647
Preprint. Discussion started: 23 June 2025

neighbour count map, where each cell of the map was assigned the closest distance to a tree and the number of trees within a 10 m radius. The 2013 and 2017 ALS point-clouds were also used to derive the density and elevation roughness, calculated from their standard deviation, of the ground points within the grid cells of the DTMs.

In addition to this, there was also a 0.1 m resolution orthophoto provided by the Federal State of Tyrol. This orthophoto was acquired using an airplane on 10 June 2015, only a few days after the investigated event. In this study, the dataset was used for validation of the landslides detected by the RF model. Lastly, for filtering bank erosion and landslides located near roads, the map of the stream network in Tyrol (Land Tirol, 2023) was used to construct a stream mask and data from the road network (ÖVDAT, 2022) was used for a road mask, both masks were constructed by applying a 15 m buffer on the datasets.

3.2 Segmentation of BFW landslide inventory and construction non-landslide area

To construct a polygon-based inventory from the existing point-based BFW inventory, a seeded region growing algorithm from SAGA GIS (v9.7.2) (Conrad et al., 2015) was used on the original dataset. The input features consisted of the DoD (original DoD downscaled to a 0.1 m resolution) and the after-event orthophoto. The delineation of the scars from the seeded region growing was checked against the orthophoto and DoD, including its slope, hillshade and topographic openness at 5 and 10 m. These derivatives are often used in landslide mapping as they can clearly delineate the edges of landslide scars (Petschko et al., 2016; Razak et al., 2011).

It was unknown how many additional landslides occurred within the 2013 to 2017 timespan. This meant that use of the full area in the training dataset for training of the RF landslide detection model could include a large number of landslides falsely classified as stable or unchanged areas within the training dataset. For this reason, it was decided to also delineate areas where no landslides were present in the DoD dataset and only use the segmented scars of the BFW inventory and this “non-landslide” area for the training of the landslide detection model. The non-landslide area was delineated after visual inspection of the orthophoto and DoD, including its slope, hillshade and topographic positive openness derivatives.

3.3 Landslide detection with RF model

For the detection of additional landslides, an RF model was trained on the segmented BFW inventory and the non-landslide area. The framework for the RF model was taken from the scikit-learn Python library (v1.5.1) (Pedregosa et al., 2011). The input of the RF model consisted of the DoD and several DoD uncertainty proxy datasets. The change estimation values from a DoD dataset come with uncertainties that result from the simplification of the original point-cloud datasets, which occurs in the construction of the underlying DTM datasets. These uncertainties can be approximated with the point density of the point-cloud and the surface roughness of the terrain (Li et al., 2024). To account for the DoD uncertainty in the landslide detection model, it was decided to use the point-density and elevation roughness of both years as additional input in the RF model. The final input of the RF model thus consisted of the DoD and four uncertainty proxy layers.

To hypertune the RF model, a set-up was created in Python using the Optuna library (v4.0.0). The Optuna library provides a framework for optimizing the search of the optimal hyperparameter combination within a large hyperparameter space (Akiba

https://doi.org/10.5194/egusphere-2025-2647
Preprint. Discussion started: 23 June 2025

et al., 2019). The value ranges used for the hyperparameter tuning are given in Table A.1 in the appendix. To optimally search the hyperparameter space, the Optuna framework fits an optimization function from the hyperparameters of previous runs and a chosen model performance metric. In this study it was decided to use the area under the curve (AUC) metric and the Jaccard index derived with three cross-validation folds for the hyperparameter optimization. The training dataset was split into three subsets for hypertuning (20%), training (48%) and testing (32%) of the model. The final hyperparameter set-up was based on the model run with the highest AUC value, the parameter values of this set-up are given in Table A.1 in the appendix.

After the RF model was hypertuned and trained, the probability output from the RF model was segmented with a separate segmentation workflow, since the classification by the RF model led to large overestimation of landslide locations. An overview of the full workflow is given in Figure A.1 in the appendix. The first step of this segmentation workflow was a segmentation and filtering of the RF probability output. The filtered probability output was then used to extract seed locations and perform seeded region growing with the seed generation and seeded region growing tools from SAGA GIS (v9.7.2). The input for the seeded region growing consisted of the RF probability, the DoD, and the average RF probability within a specific windowsize. The region growing resulted in several smaller segments with similar probability values. In a next step, these segments were clumped together with the r.clump algorithm from GRASS GIS (v7.8) (GRASS Development Team, 2024) based on their average probability. These clumped segments were then filtered based on their size and average probability.

Since the full workflow required a large number of parameters, it was decided to also use the Optuna optimization workflow for their optimization. The full list of parameters and their final calibration values are given in Table A.2 in the appendix. The optimization in Optuna for the segmentation workflow was based on the distance to the perfect classification (D2PC) and Jaccard index. Since the filtering of false positives was deemed more important than a detection of all the occurred landslides, the decision of the best parameter set-up was based on the Jaccard index.

3.4 Mapping of additional scars from RF detection

The final step of the RF inventory construction was mapping the landslide scars within the detected landslide area by the RF model. For this, the convergence index from SAGA GIS (v9.7.2) was used to detect sink and peak areas within the DoD dataset. Since the scars of the landslides are represented as distinct sinks within the DoD data, a negative threshold on the convergence index was used to map the landslide scar areas. A visual inspection of the convergence index at different threshold levels showed that a threshold of -30% was best at separating the scar areas from secondary erosion zones, such as gully erosion, while also preserving the size of the landslide scar. After the best threshold was selected, the convergence index was segmented and each of the segments overlapping with the landslide detection output were validated. Only the segments showing landslides signs in the DoD or orthophoto were kept in the final inventory. Outliers of underestimated scar segments, where the convergence index only captured a steep pit within the landslide scar, were filtered out using the minimum scar size from the BFW inventory.

https://doi.org/10.5194/egusphere-2025-2647
Preprint. Discussion started: 23 June 2025

3.5 Morphological and topographic profile analyses of the scars and their forest cover

The main goal in the analysis of the RF scars was to investigate the differences between landslides within the forest and those located outside the forest. To achieve this, the scars first had to be classified according to their forest canopy cover. If a scar segment was covered for 90% or more by the constructed canopy cover mask, the scar was classified as located within the forest. If the scar did not have any cover by the constructed canopy cover mask it was classified as located outside the forest. To create a better distinction between landslides within and outside of the forest, landslides with partial cover < 90% were excluded from this binary analysis. To analyse the relationship between the forest structure and the characteristics of the landslides, additional analyses were also performed based on a tree distance map and a map of the tree count within a 10 m radius from each cell. These maps were used to extract the average distance to the closest tree and the average number of trees within a 10 m radius from the cells within each of the scars. This analysis also included the landslides with partial forest cover < 90%.

Both the forest classification and the parameters with information on the trees surrounding the scars were then used to investigate their relationships with the morphological characteristics of the scars. The analysed morphological scar parameters were the scar area (A), scar depth (D), scar thickness (T), scar volume (V), scar length (L), scar slope and ratios of the scar length with its mean depth (D_{mean}/L) and thickness (T_{mean}/L). An overview of these parameters, their abbreviations and sources is given in Table 1. To extract the landslide thickness, which in this study is defined as the distance from the original topography to the landslide slip surface in the normal direction, an additional topographic distance map was constructed from the two DTMs with the M3C2 method from Cloudcompare (v2.14) (Lague et al., 2013). Additionally, a line along the aspect direction of the slopes was also used to extract the scar length. The length parameter was used to derive the ratios of the scar depth and thickness with its length. These are all parameters that are often used in the analysis of landslides (Rickli and Graf, 2009; Schaller et al., 2025; Zieher et al., 2016). Besides a visual inspection of the relationship of these parameters with the forest parameters using boxplots and scatter plots, the statistical relevance of their relationship was also investigated with a Wilcoxon-Withney U test and Welch's t-test for the binary classification of the scars according to their forest classification. The relationships with the distance to the closest tree parameter and the parameter describing the number of trees in the vicinity of the scar were analysed with analysis of variance (ANOVA) tests. All statistical test set-ups were taken from standard set-ups in the scipy (v1.15.1) Python library (Virtanen et al., 2020).

The landslide topographic profiles were analysed by extracting the thickness of the landslides along profile lines within the landslides. To enable a comparison between the different scars, two profile lines with fixed length were drawn through the centroids of the scars along the average aspect direction within the scar and perpendicular to this aspect direction. To compare the thickness profiles from the scars inside and outside of forests, the median and the inter-quartile range (IQR) of the thickness was calculated for each classification along the extracted profiles. Differences between the median thickness profiles were quantified by calculating the root mean squared deviation of the median profiles along segments of the profiles.

https://doi.org/10.5194/egusphere-2025-2647
Preprint. Discussion started: 23 June 2025

Table 1: Overview of the morphological parameters, their abbreviations and the source of their construction.

Parameter name	Abbreviation	Source	Unit
Scar volume	V	Sum of the DoD values in the scar	m^3
Scar area	A	Area of the scar from the number of scar cells	m^2
Scar length	L	Length of the mean aspect line intersecting the scar	m
Scar slope	-	Average slope of the 2013 DTM in the scar	°
Scar depth	D_{mean} or D_{max}	Mean and min. DoD values in the scar	m
Scar thickness	T_{mean} or T_{max}	Mean and min. M3C2 distance values in the scar	m
Thickness length ratio	T_{mean}/L	Ratio of the mean thickness and scar length	-
Depth length ratio	D_{mean}/L	Ratio of the mean depth and scar length	-

4 Results

4.1 Landslide detection based on the RF model and scar extraction

The probability output from the RF detection model is shown for two example areas in Figure 4i and Figure 4j. The model performance of the final RF model has a Jaccard index of 0.049 and an AUC value of 0.94, tested with the hypertuning dataset. The ROC-curves of the random forest model on the testing and training datasets are given in Figure 5a. Using the testing dataset and with a filter of the probability output on the threshold with the best D2PC value of 0.19, the TPR and FPR are 85% and 13%, respectively. Note that these performance metrics are calculated on a pixel-basis.

An analysis of the feature importance of the trained random forest model is given in Figure 5b. The feature importance was assessed with the sci-kit learn Python library through permutation of the individual features of the model input and assessing the impact of this permutation on the model performance, in this study the AUC score. The results show that, as expected, the DoD has the largest impact on the model performance with an average drop in AUC of 0.20. After the DoD, the roughness of the 2017 data has the largest impact on the model performance, followed by the roughness of the 2013 data. Respectively, they result in an average a drop in AUC of 0.03 and 0.02 after their permutations. The point-density layers of 2017 and 2013 see an average drop of 0.006 and 0.004, respectively. It should be noted with this analysis that the point-density and roughness datasets are related to each other and a univariate analysis results in biased statistics, which could lead to lower values of feature importance for these layers.

Since the classification results of the RF model resulted in a high degree of overestimation, also in terms of number of landslides, it was decided to apply an additional filtering and segmentation algorithm to the probability output of the RF model. The results from this are given in Figure 4. The trained algorithm has a Jaccard score of 0.52 and a D2PC value of 0.26. The false positive rate is only 0.18%, with a TPR of 73.8%. Note that these performance metrics are also calculated on a pixel-basis. A manual check of each of the segmented polygons resulted in 54% true positives on an object-basis. 45% of the

https://doi.org/10.5194/egusphere-2025-2647
Preprint. Discussion started: 23 June 2025

270 polygons were deemed false positives. The results from the final output of the landslide detection algorithm are also shown in Figure 4.

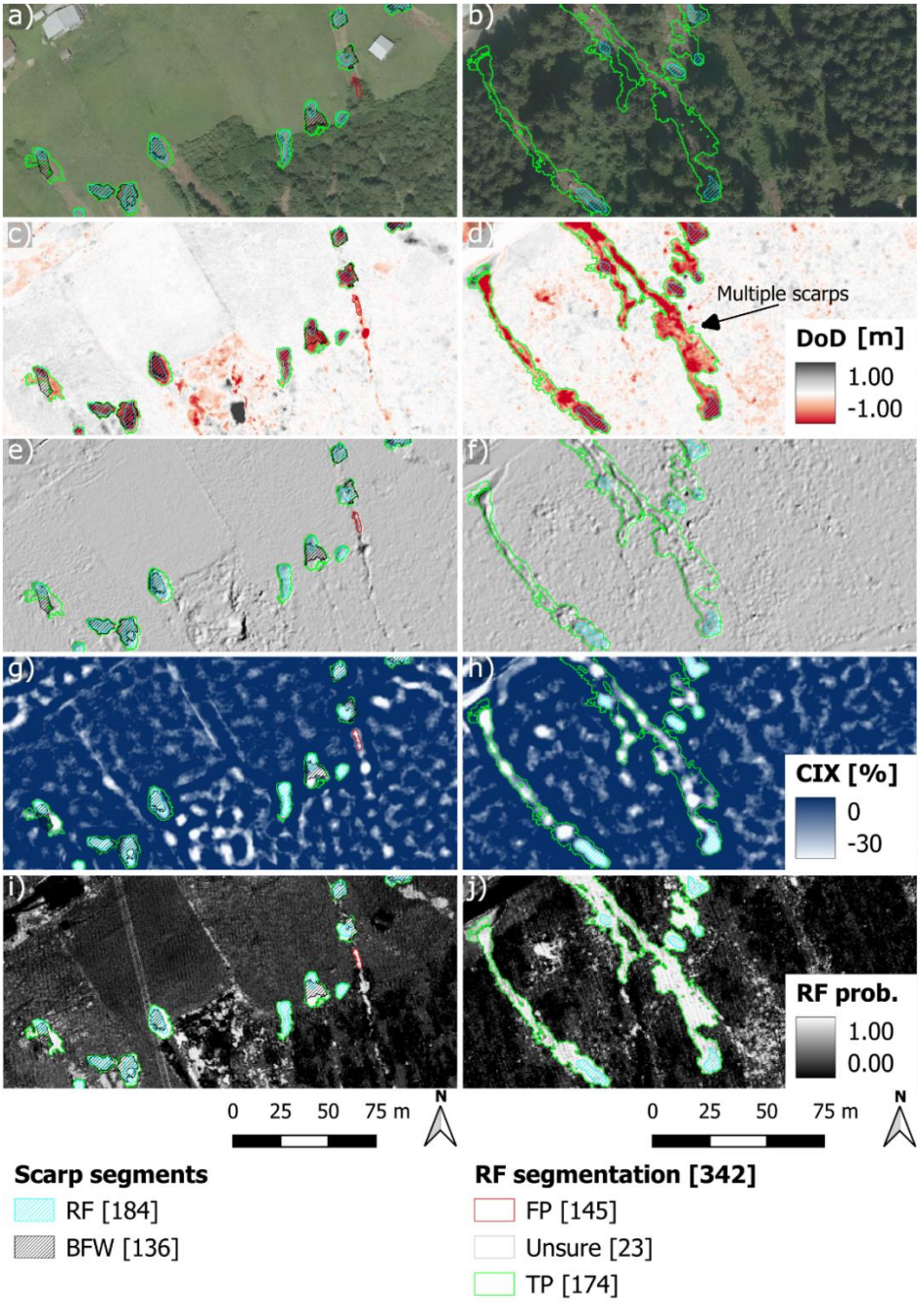

Figure 4: Output of the RF segmentation and subsequent scar mapping compared with the original BFW inventory for two example areas, shown on the post-event orthophoto (a, b), the DoD (c, d), a hillshade of the DoD (e, f) (all three base layers 275 **provided by the federal state of Tyrol), the convergence index (CIX) used in the scar mapping (g, h) and the probability output of the RF model (i, j).**

https://doi.org/10.5194/egusphere-2025-2647
Preprint. Discussion started: 23 June 2025

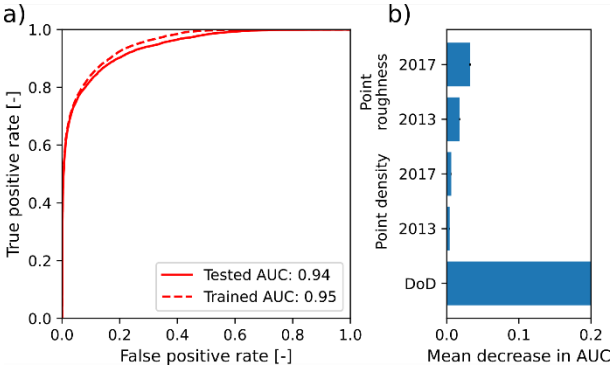

Figure 5: ROC curve of trained RF detection model (a) and feature importance of the input features, measured as mean decrease in AUC value (b).

After mapping the scars in the detected landslide areas with the convergence index, 184 landslides were found of which 51 are covered for more than 90% by the canopy cover mask. 65 landslides intersect with a landslide in the BFW inventory. An analysis of the BFW landslides that were not detected by the RF inventory showed that a large number was either located on the debris flood deposit or too shallow to leave signs in the DoD data. Thus, the RF model found 119 additional landslides. A summary on the landslide characteristics from both the RF and BFW inventories is given in Table 2. The plots in Figure 6 show the relationships of the landslide scar areas with their volume (Figure 6b) and mean depth (Figure 6c), for the original BFW and new RF inventories. It is interesting to note that both inventories mainly consist of shallow landslides, with mean depths below 2 m for most of the scars. In addition, it is also interesting to note that the relationship of the landslide volume and area in the RF inventory is very linear, while for the BFW inventory the relationship is more spread with a larger range of landslide depths for different scar sizes.

The plot in Figure 6a shows the frequency density distribution for the scar areas of the RF and segmented BFW inventories. The plot shows that as proposed in Malamud et al. (2004), the landslides follow a power-law distribution with a drop of in frequency for the smallest scar areas. What should be noted is that the distributions of both the RF and BFW inventories are quite different from the Malamud distributions with a shift to lower area sizes with a factor 20. However, it should be noted that the inventories analysed in Malamud et al. (2004) consider the full process area, while the constructed inventory in this study only considers the scar area.

It is clear from these figures that both datasets contain outliers. The distributions in Figure 6 and the statistics in Table 2 also indicate that some of the landslides in the RF inventory have a very small scar area < 3 m^2. Additionally, the BFW inventory also contains several landslides located on the debris flood deposit, which results in negative mean depth and volume estimates from the DoD data. These landslides were filtered out with the outlier filter and they are not considered in the remaining analyses.

https://doi.org/10.5194/egusphere-2025-2647
Preprint. Discussion started: 23 June 2025

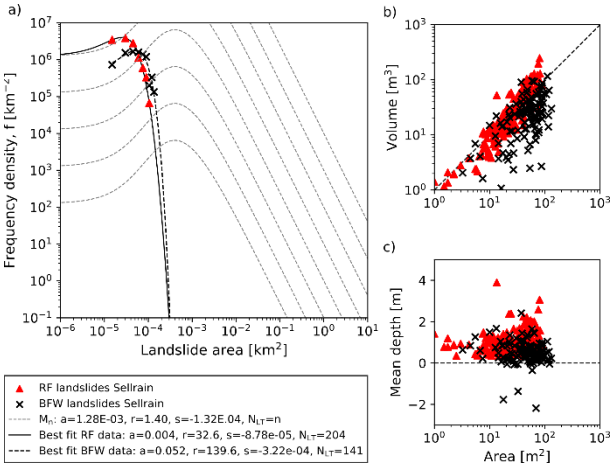

Figure 6: Frequency density distributions of the BFW (in black) and RF (in red) scar areas (a). No outlier filter was applied to the data. The fitted curves are fitted according to the Malamud distribution, of which the standard distributions are also given as grey dotted lines for different landslide inventory sizes. The plots on the right show the relationship of the scar areas with their volume (b) and with their mean depth (c).

Table 2: Summary statistics of the RF and BFW inventories with mean scar areas, mean DoD values, mean scar volumes, total scar count and scar count after the filtering step. The statistics are also calculated on just the landslides within the forests and outside the forest.

	Full inventory					Within forest					Outside forest			
	Area	*DoD*	*Volume*	*Count*		*Area*	*DoD*	*Volume*	*Count*		*Area*	*DoD*	*Volume*	*Count*
				All	*Filtered*				*All*	*Filtered*				*All*
RF	28.3	-1.0	33.0	184	174	26.0	-1.2	35.0	51	48	27.1	-1.0	28.4	114
BFW	52.1	-0.3	21.5	132	119	29.2	-0.8	23.2	16	15	55.9	-0.2	20.0	102

4.2 Morphological and topographic profile analysis of the RF scars in forests and outside of forests

Comparisons of the morphological parameter distributions of the scars in the RF inventory are given in Figure 7, with a statistical summary given in Table 3. The comparison of the mean depth distributions shows that there is a difference between the mean depth values of the scars in the forests and those outside the forest, with respective average "mean depth" values of 1.2 m and 1.0 m. Another difference is found in the D_{mean}/L ratio of the scars and the slope of the pre-event DTM (Figure 7f and Figure 7h). In the forest the D_{mean}/L ratio is on average 0.24 and the pre-event slope 40.8°, while outside the forest the average D_{mean}/L ratio is lower at 0.18 and the slope values are also lower with an average of 38.5°. Smaller differences are also found in the mean thickness of the scars, with respective average values of 0.8 and 0.7 m inside and outside the forest. Similarly, the maximum thickness values of the scar are higher in the forest with a value of 1.0 m against a value of 0.8 m outside the forest. Lastly, the T_{mean}/L ratios of the scars also show a slight difference with a value of 0.15 inside the forest against a value of 0.12 outside the forest.

When these differences are analysed to derive their statistical relevance (Table 3), both the Mann Withney U test and Welch's t-test show that the differences in scar depth, D_{mean}/L ratio and slope of the pre-event DTM are statistically significant with p-values < 0.05. The differences in scar thickness and T_{mean}/L ratio are statistically significant with p-values < 0.10. The

https://doi.org/10.5194/egusphere-2025-2647
Preprint. Discussion started: 23 June 2025

differences between the volume and area statistics inside and outside the forest are smaller and not statistically significant according to the Mann Withney U test and Welch's t-test.

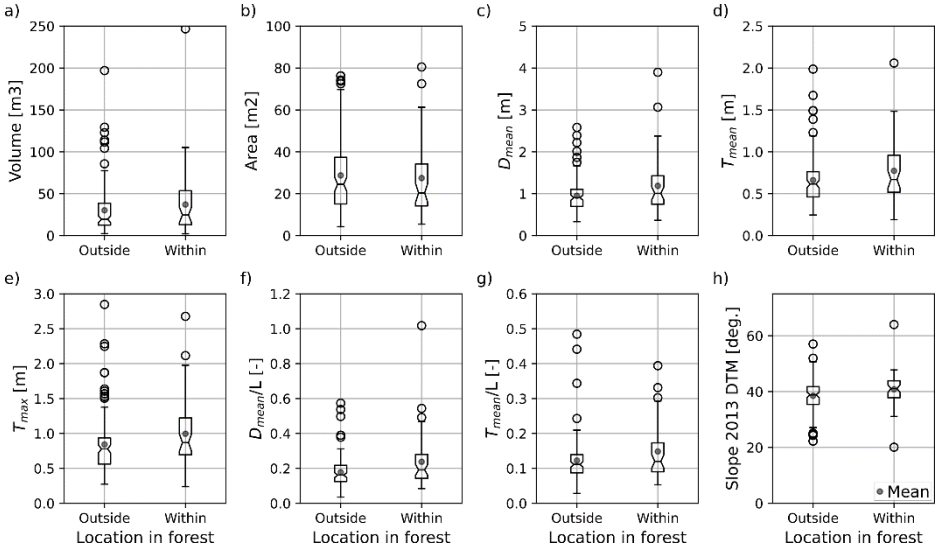

Figure 7: Distributions of the morphological scar parameters in the RF inventory visualized as boxplots with a grouping according to the landslide forest cover (within or outside the forest). The plotted parameters are the (a) scar volume, (b) scar area, (c) the mean scar depth, (d) the mean scar thickness, (e) the max. scar thickness, (f) the mean depth/length ratio, (g) the mean thickness/length ratio and (h) the average slope in the 2013 DTM.

Table 3: Statistical summary of the morphological parameter distributions for the scars inside and outside the forest with the statistical significance of the differences calculated with the Mann-Withney U test and Welch's t-test.

		Forest classification scars		Statistical significance	
		Within Forest	Outside Forest	Mann-Witney U test	Welch's t-test
Volume [m³]	*Average*	37.1	30.2	0.445	0.307
	Std. dev.	40.9	30.8		
Area [m²]	*Average*	27.5	28.7	0.556	0.680
	Std. dev.	17.8	17.7		
D_{mean} [m]	*Average*	1.2	1.0	0.030	0.027
	Std. dev.	0.7	0.4		
T_{mean} [m]	*Average*	0.8	0.7	0.081	0.083
	Std. dev.	0.4	0.3		
T_{max} [m]	*Average*	1.0	0.8	0.060	0.079
	Std. dev.	0.5	0.4		
D_{mean}/L [-]	*Average*	0.24	0.18	0.019	0.019
	Std. dev.	0.16	0.09		
T_{mean}/L [-]	*Average*	0.15	0.12	0.105	0.061
	Std. dev.	0.08	0.07		
Slope [°]	*Average*	40.8	38.5	0.013	0.027
	Std. dev.	5.95	5.92		

https://doi.org/10.5194/egusphere-2025-2647
Preprint. Discussion started: 23 June 2025

Figure 8 shows how the average closest tree distance within the scar relates to the different morphological parameters. The plots show that there is a relationship between the average closest tree distance and the mean scar depth, the mean scar thickness and the maximum scar thickness, with larger distances of the closest tree relating to smaller scar thicknesses and depths. Figure 8d also shows a strong relationship between the average distance to the closest tree and the scar D_{mean}/L and T_{mean}/L ratios. Lastly, the boxplots on top of each of the subfigures also indicate that there is a strong relationship between the distance to the trees and the slope of the pre-event DTM. An ANOVA on the formed groups from the plots in Figure 8, also shows that except for the volume and area parameters, the differences in parameters between the groups is statistically significant with p-values from the ANOVA all falling below 0.05 (Table 4).

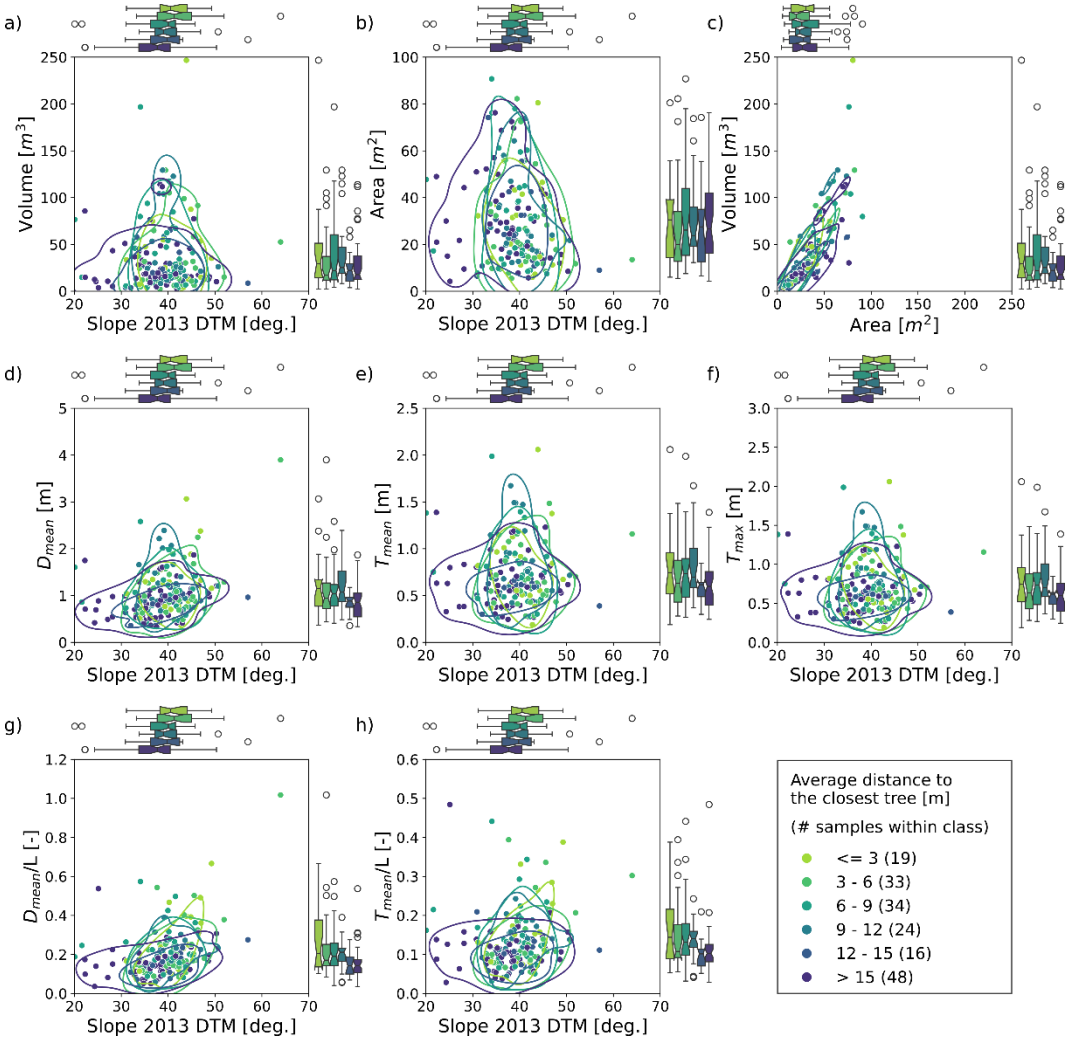

Figure 8: Analysis of the relationship between the scar area and average slope of the scars from the 2013 DTM data, coloured by the average closest tree distance within the scar. The contour boundaries show the 75th percentile boundary of the binned tree distance subsets. The plotted parameters are (a) the scar volume, (b) the scar area, (c) the scar volume against the scar area (instead of the 2013 DTM slope), (d) the mean depth, (e) the mean thickness, (f) the maximum thickness, (g) the mean depth to length ratio and (h) the mean thickness to length ratio.

https://doi.org/10.5194/egusphere-2025-2647
Preprint. Discussion started: 23 June 2025

Table 4: Results ANOVA on the grouped data and parameters from Figure 8.

	p-values ANOVA
Volume	0.354
Area	0.945
D_{mean}	0.0154
T_{mean}	0.0268
T_{max}	0.0185
D_{mean}/L	0.0045
T_{mean}/L	0.0149
Slope	0.0093

Figure 9 shows similar results but uses the average number of trees within a 10 m radius for each of the scar cells to group the data. The analysis shows that there is only a difference between the group that on average has no neighbouring trees and the other groups. If the group without trees would be filtered out, the groupings would not show any differences. This was also shown with ANOVA tests on the different parameters, using a filtered dataset where the group without trees was left out. The p-values of these ANOVA tests all fell above 0.05, including for an ANOVA test on the relationship with the 2013 slope of the scar.

https://doi.org/10.5194/egusphere-2025-2647
Preprint. Discussion started: 23 June 2025

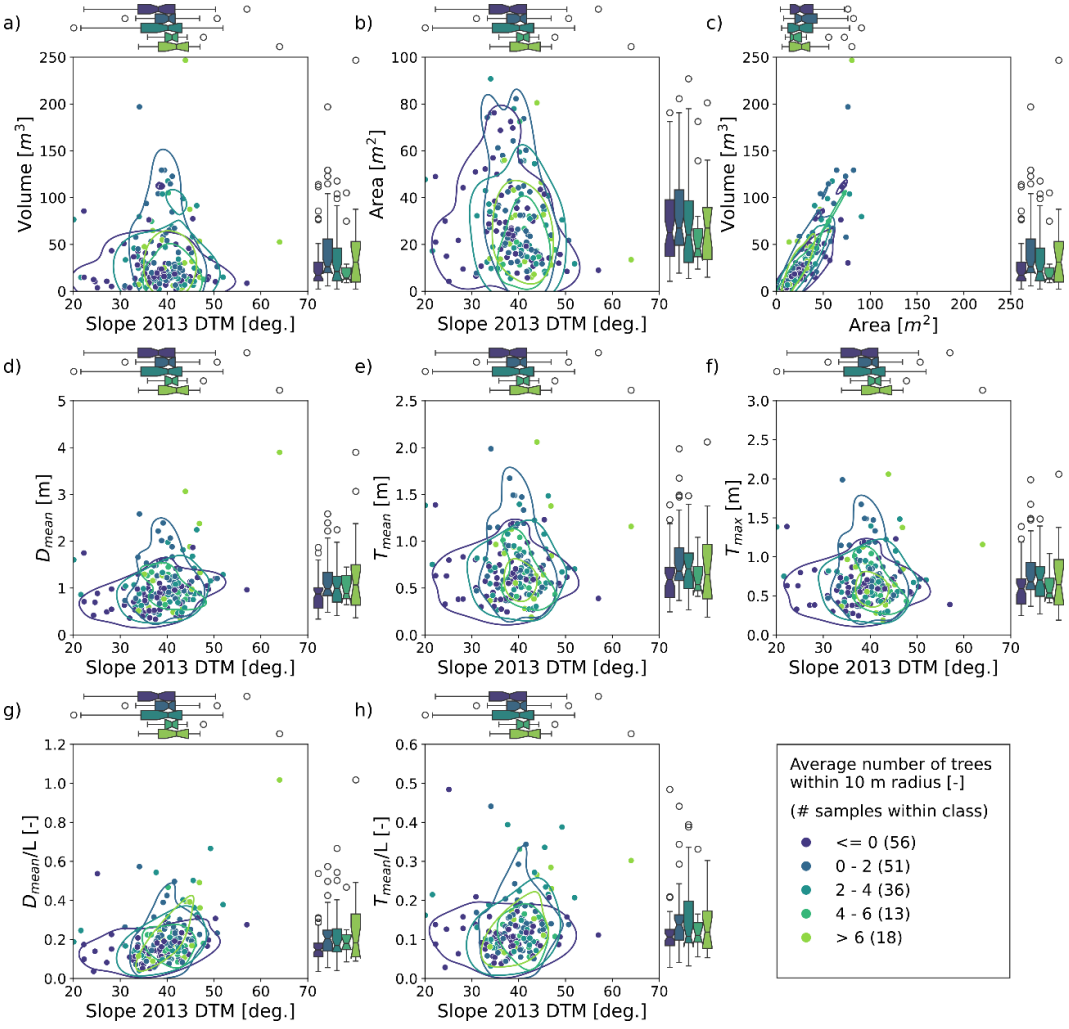

355 **Figure 9: Analysis of the relationship between the scar area and average slope of the scars from the 2013 DTM data, coloured by the average number of trees within a 10 m radius for each of the scar cells. The contour boundaries show the 75th percentile boundary of the binned average tree number subsets. The plotted parameters are (a) the scar volume, (b) the scar area, (c) the scar volume against the scar area (instead of the 2013 DTM slope), (d) the mean depth, (e) the mean thickness, (f) the maximum thickness, (g) the mean depth to length ratio and (h) the mean thickness to length ratio.**

360 The analysis of the landslide topographic profiles with regards to its forest classification is given in Figure 10. The plots of the topographic profiles along and across the slopes show that the median thickness profile of the landslides in forests is deeper than the thickness profile of the landslides outside the forest. The difference in the profiles of the thickness data is especially clear in the across-slope profiles. In addition to the general difference in thickness, the along-slope profile also indicates that the scar head profile of the landslides within the forest is generally steeper than from landslides outside the forest. Within the 365 interval of -7 to 7 m, the median across slope profiles have a root mean squared deviation (RMSD) of 0.08 m. For the interval -2 to 2 m this increases to 0.12 m. For the along the slope profiles, the difference of the median profiles has a RMSD value of 0.07 m for the interval -7 to 15 m. For the interval -2 to 2 m, this increases to 0.09 m.

https://doi.org/10.5194/egusphere-2025-2647
Preprint. Discussion started: 23 June 2025

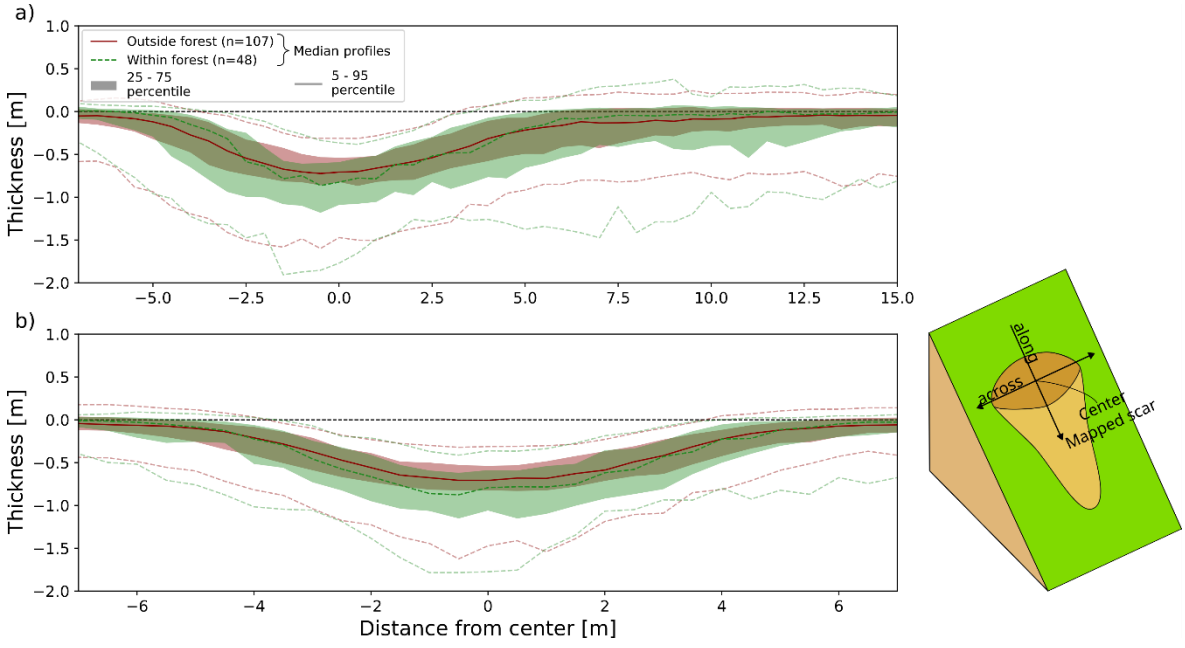

Figure 10: Topographic profiles from the thickness dataset of the scars within the forest (green) and outside the forest (red) along the aspect direction (a) and across the aspect direction (b). The x-axis indicates how far the point of the profile is located from the centroid of the scar.

Lastly, Figure 11 shows the relationship between the topographic profiles of the landslides and the average closest tree distance and the slope of the pre-event DTM. The graphs show that both the slope and the average tree distance have an impact on the profiles of the landslides. With a smaller average closest tree distance, the landslide profile is generally deeper than with larger tree distance values. For the slope of the pre-event DTM, the plots show that a larger slope value is generally related to deeper landslide profiles and smaller slope values to shallower landslide profiles.

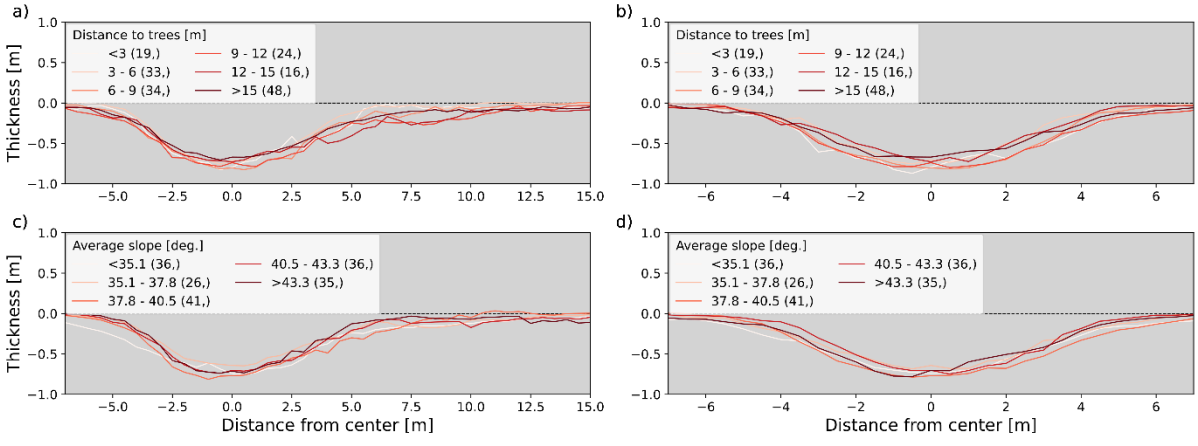

Figure 11: Median profiles from the thickness dataset with a grouping of the landslide according to their average closest tree distance (a, b) and the average slope in the 2013 DTM (c, d). The plots on the left (a, c) show the landslide profiles along the aspect and the plots on the right (b, d) the profiles across the aspect.

https://doi.org/10.5194/egusphere-2025-2647
Preprint. Discussion started: 23 June 2025

5 Discussion

5.1 Performance of the landslide detection and scar mapping with the RF model

The performance metrics show a good performance of the RF model (AUC: 0.94) and the subsequent segmentation of the RF output (D2PC: 0.26 with TPR of 73.8%). The metrics show that there is a general underestimation of the landslide area and occurrence in the final inventory, however, this is traded off with a very low false positive rate. Since one of the main goals in developing the RF workflow was a higher degree of automation, a lower false positive rate was preferred over a higher true positive rate. A lower false positive rate also ensures that a higher certainty can be attached to the final inventory.

The degree of automation was a very important focus in the creation of the landslide scar detection and segmentation workflow. A higher degree of automation also brings with it a better transferability and a higher robustness of the results from the statistical analysis, since with it the impact of human decision-making or errors on the analysis is also lowered. It was not possible to create a fully automated workflow, as the output of the detection and segmentation workflows still had high false positive rates. The human intervention within the developed workflow was limited to only the exclusion or inclusion of certain landslides. Since the output from the convergence index was used directly in the scar representation, the human intervention did not change the scar boundaries.

With regards to the validity of the scar boundaries in this study, it should be said that although there might be some discrepancies in the delineation of scars in our approach compared to more traditional landslide mapping approaches, the effects of these discrepancies do not affect the conclusions in the comparison of landslides within and outside of the forest. It can be assumed that the under- and overestimation of the scar sizes is consistent across the different forest classifications. In addition, it should also be pointed out that the found differences in the landslide profiles and depth derivatives are not affected by the scar construction.

5.2 Morphological and topographic profile differences of landslides within and outside of forest in the RF inventory

The distributions of the morphological landslide parameters and the topographic profiles of the scars in the RF inventory, showed that there are distinct differences between landslides in the forest and landslides located outside forests. From the morphological characteristics it was shown that there is a statistically significant difference in the slope of the scars in the pre-event DTM, the depth of the scars and their D_{mean}/L ratios, with significantly higher slopes, deeper scars and higher D_{mean}/L ratios for landslides located within the forest. It should be noted that the higher slope angle was expected due to prevalence of steeper slopes within the forest in the study area. The analysis also showed that to a lesser degree the scars are also different when the thickness is considered instead of the depth, with similar results of larger thickness values and larger T_{mean}/L ratios for scars located in the forest. No relationship was found between the area and volumes of the scars and their location respective to the forest. This is also supported by the more detailed analysis of the relationship of the morphological parameters with the average tree distance within the scar. This analysis showed that there is a relationship between the thickness and depth related parameters and the proximity of trees to the scar. The plots of the topographic profiles of the scars also showed that the scar

https://doi.org/10.5194/egusphere-2025-2647
Preprint. Discussion started: 23 June 2025

thickness is larger for landslides located closer to trees. Interestingly, these plots also showed that the along-slope profile of the scars in the forest is steeper than those from scars outside the forest, suggesting that the scar length of these scars is also shorter. The analysis investigating the relationship of these differences with the number of trees within the scar neighbourhood (Figure 9), showed that the found differences are only related to the presence of trees within a certain radius. This indicates distance to trees surrounding the scar has a stronger relationship with the scar characteristics than the number or density of trees surrounding the scar.

However, it is unclear from the results if the relationship between the found larger scar depths and larger depth/length ratios is related to the presence of a forest around the scar or the larger slope angles of the terrain within the forest, which also impacts the mechanics and thus the morphological and topographic profile characteristics of the landslide. In addition to the differences in slope characteristics, it is also unknown whether other differences between the scars inside and outside the forest, unrelated to the forest cover, are influencing the found differences. Examples of this could be difference in soil type or soil structure, which could influence the geotechnical and hydrological conditions of the soil. In addition, it should also be noted that the profiles could reflect differences in erosional processes that occurred after the event. A more detailed field study or remote sensing analysis of the forests within the study area would be needed to answer these questions more conclusively. Besides additional data on the forest and soil properties in the study areas this would also require a larger dataset of landslides, most likely needing data from multiple study areas to meet the size requirements of this landslide dataset.

5.3 Landslide characteristics in other studies

The areas of the scars in this study are significantly lower than what is reported in other studies (Emberson et al., 2022; Malamud et al., 2004). However, this discrepancy is expected due to the different approach that was used for the landslide mapping in this study. Most studies reporting statistics on landslides constructed their inventories from aerial or satellite imagery. Besides this, the decision on which sections of the landslides (only the scar, the full erosional area or also the depositional area) are included within the landslide boundary can vary significantly across the different studies (Guzzetti et al., 2012). In addition, most inventories also do not focus on a specific landslide type and include both large deep-seated landslides as well as small shallow landslides (Reichenbach et al., 2018). This makes it very difficult to compare information on landslide parameters across different studies and has also been reported before by other studies (Ardizzone et al., 2007; Zieher et al., 2016). Within the current study this problem is also displayed by the differences of the BFW and RF inventories.

With regards to the comparison of landslides within and outside of the forest, a study by Roering et al. (2003) shows that the root cohesion is highly related to the spacing, size and condition of trees and thus the location of landslides, in agreement with the found importance of the tree distance parameter in the current study. Only a few studies provide insight into how the forest cover affects other landslide characteristics. Rickli & Graf (2009) compared the area, depth and volume values of landslides in forests and outside of forests from multiple study sites in Switzerland. They did not find consistent results about the area, volume and depth parameters, as the direction and significance of differences in area, volume and depth between landslides inside and outside of forests varied across the different study sites. Koyanagi et al. (2020) investigated earthquake induced

https://doi.org/10.5194/egusphere-2025-2647
Preprint. Discussion started: 23 June 2025

landslides and found that forested landslides are smaller than those outside the forest. In addition, they also found that forested landslides are deeper than those outside the forest. They did not test the significance of these differences. However, the difference in landslide depth within the forest was more than 2 times the mean landslide depth outside of the forest for one of the sites. It could be that these differences in landslide depth for forested landslides found by Koyanagi et al. (2020) are related to the difference in processes behind earthquake triggered and rainfall-triggered landslides. Additionally, it should also be noted that comparability across studies is limited in extend since no standardized forest definitions are used.

6 Conclusions

In this study we developed a well performing semi-automatic landslide detection and mapping workflow that also explicitly considers landslides under forest canopy cover. The main aim of this study was to use this semi-automatic workflow for the analysis of landslides in forests and the effect of the forest cover on the landslide morphology and topographic profiles. To analyse this, the study used an extreme short-burst rainfall event that triggered a large number of shallow landslides in the Sellrain valley, Tyrol (Austria). The results of the analysis show that there are significant differences between landslides inside and outside of forests for the studied event, with significantly larger depths, larger thicknesses and higher pre-failure slope values for landslides located in forests. An analysis with forest structure parameters (i.e., the distance to the closest tree and the number of trees within a 10 m neighbourhood radius) also showed that these differences were mainly related to the distance to the closest tree. Furthermore, the analysis showed that the found differences become clearer when the forest structure is considered, indicating that it is important to include such forest structure parameters in the research of forested landslides.

It was possible to determine there are significant differences landslides within and outside of the forest, however, determining what processes are underlying these differences would require data from more well-documented events, including comprehensive soil and forestry information. Since the current study already showed a strong link between the distance to the closest tree and the landslide characteristics, further research could focus on how the threshold of this distance is impacted by different soil types and if different tree species also show different distance thresholds. In conclusion, the results provide a better understanding of the roles of forests and how they affect the processes behind shallow landslides.

https://doi.org/10.5194/egusphere-2025-2647
Preprint. Discussion started: 23 June 2025

Appendix

The hyperparameter set-up for the RF landslide detection model is given in Table A.1. The final optimal hyperparameter set-up is also given in this table and was chosen after 300 trials based on the highest AUC score, resulting in a more balanced model performance.

The workflow for the segmentation algorithm that was applied to the probability output of the RF detection model, for further false positive filtering, is given in Figure A.1. The set-up for the paramter ranges is given in Table A.2. The parameters were also tuned with Optuna and the final parameter combinations were chosen after 1200 model runs, based on the highest D2PC value. The final parameter values are also given in Table A.2.

Table A.1: Tuned hyperparameters for the random forest landslide detection model with the used ranges and the final values.

Hyperparameter	Sampling scale	Range	Final value
Maximum tree depth	Linear	[2 - 80]	37
Minimum leaf samples	Logarithmic	[1e-5 – 0.3]	0.000044
Minimum split samples	Logarithmic	[1e-5 – 0.3]	0.005164
Number of estimators	Logarithmic	[5 – 400]	206

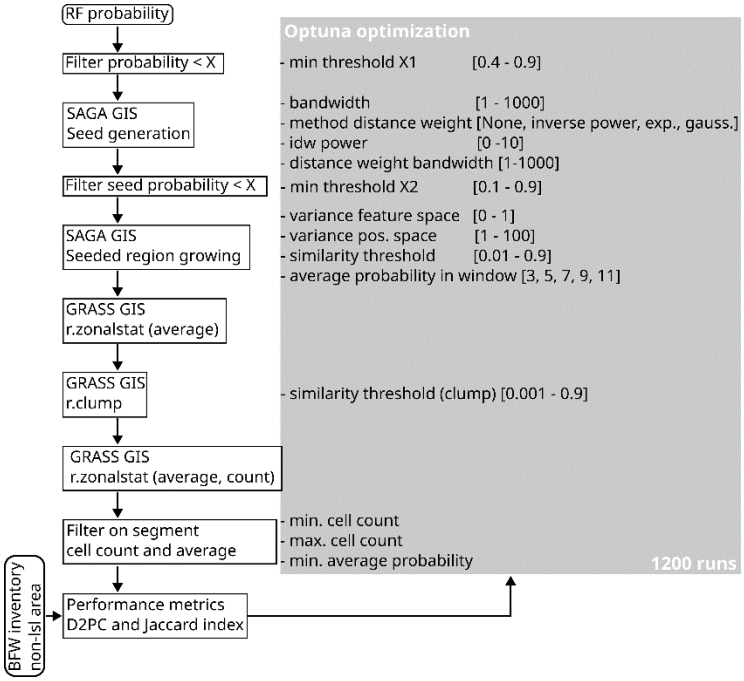

Figure A.1: Workflow for segmentation and filtering of the probability output of the random forest landslide detection model.

https://doi.org/10.5194/egusphere-2025-2647
Preprint. Discussion started: 23 June 2025

Table A.2: Overview of the parameters used in the segmentation workflow, with the final values given in the rightmost column.

	Workflow step	Sampling scale	Range	Final value
Minimum probability	Filter RF probability	Linear	[0.4 – 0.9]	0.84
Bandwidth	Seed generation	Logarithmic	[1 – 1000]	2.78
Distance weighting method	Seed generation	Categorical	[None, inverse power, exponential, gaussian]	Inverse power
IDW power	Seed generation	Linear	[1 – 10]	5.22
Weighting bandwidth	Seed generation	Logarithmic	[1 – 1000]	[-]
Seeds probability threshold	Filter seeds	Linear	[0.1 – 0.9]	0.89
Variance feature space	Seeded region growing	Linear	[0.0 – 1.0]	0.66
Variance position space	Seeded region growing	Logarithmic	[1 – 100]	5.31
Similarity threshold seeds	Seeded region growing	Logarithmic	[0.01 – 0.90]	0.06
Windowsize average probability	Seeded region growing [input]	Categorical	[3, 5, 7, 9, 11]	5
Similarity threshold	r.clump	Logarithmic	[0.001 – 0.900]	0.70
Minimum segment size	Final segment filtering	Logarithmic	[1 – 1000]	65
Maximum segment size multiplication factor	Final segment filtering	Logarithmic	[1.1 – 20000] * min. segement size	11574
Average probability of segment threshold	Final segment filtering	Linear	[0.3 – 0.9]	0.82

485

https://doi.org/10.5194/egusphere-2025-2647
Preprint. Discussion started: 23 June 2025

References

Adams, M. S., Fromm, R., and Lechner, V.: HIGH-RESOLUTION DEBRIS FLOW VOLUME MAPPING WITH UNMANNED AERIAL SYSTEMS (UAS) AND PHOTOGRAMMETRIC TECHNIQUES, ISPRS - Int. Arch. Photogramm. Remote Sens. Spat. Inf. Sci., XLI-B1, 749–755, https://doi.org/10.5194/isprsarchives-XLI-B1-749-2016, 2016.

Akiba, T., Sano, S., Yanase, T., Ohta, T., and Koyama, M.: Optuna: A Next-generation Hyperparameter Optimization Framework, in: Proceedings of the 25th ACM SIGKDD International Conference on Knowledge Discovery & Data Mining, New York, NY, USA, 2623–2631, https://doi.org/10.1145/3292500.3330701, 2019.

Ardizzone, F., Cardinali, M., Galli, M., Guzzetti, F., and Reichenbach, P.: Identification and mapping of recent rainfall-induced landslides using elevation data collected by airborne Lidar, Nat. Hazards Earth Syst. Sci., 7, 637–650, https://doi.org/10.5194/nhess-7-637-2007, 2007.

Brardinoni, F. and Church, M.: Representing the landslide magnitude–frequency relation: Capilano River basin, British Columbia, Earth Surf. Process. Landf., 29, 115–124, https://doi.org/10.1002/esp.1029, 2004.

Cardinali, M., Galli, M., Guzzetti, F., Ardizzone, F., Reichenbach, P., and Bartoccini, P.: Rainfall induced landslides in December 2004 in south-western Umbria, central Italy: types, extent, damage and risk assessment, Nat. Hazards Earth Syst. Sci., 6, 237–260, https://doi.org/10.5194/nhess-6-237-2006, 2006.

Cohen, D. and Schwarz, M.: Tree-root control of shallow landslides, Earth Surf. Dyn., 5, 451–477, https://doi.org/10.5194/esurf-5-451-2017, 2017.

Conrad, O., Bechtel, B., Bock, M., Dietrich, H., Fischer, E., Gerlitz, L., Wehberg, J., Wichmann, V., and Böhner, J.: System for Automated Geoscientific Analyses (SAGA) v. 2.1.4, Geosci. Model Dev., 8, 1991–2007, https://doi.org/10.5194/gmd-8-1991-2015, 2015.

Emberson, R., Kirschbaum, D. B., Amatya, P., Tanyas, H., and Marc, O.: Insights from the topographic characteristics of a large global catalog of rainfall-induced landslide event inventories, Nat. Hazards Earth Syst. Sci., 22, 1129–1149, https://doi.org/10.5194/nhess-22-1129-2022, 2022.

Eysn, L., Hollaus, M., Schadauer, K., and Pfeifer, N.: Forest Delineation Based on Airborne LIDAR Data, Remote Sens., 4, 762–783, https://doi.org/10.3390/rs4030762, 2012.

Fiorucci, F., Cardinali, M., Carlà, R., Rossi, M., Mondini, A. C., Santurri, L., Ardizzone, F., and Guzzetti, F.: Seasonal landslide mapping and estimation of landslide mobilization rates using aerial and satellite images, Geomorphology, 129, 59–70, https://doi.org/10.1016/j.geomorph.2011.01.013, 2011.

Galli, M., Ardizzone, F., Cardinali, M., Guzzetti, F., and Reichenbach, P.: Comparing landslide inventory maps, Geomorphology, 94, 268–289, https://doi.org/10.1016/j.geomorph.2006.09.023, 2008.

GeoSphere Austria: INCA hourly data [data set], https://doi.org/10.60669/6akt-5p05, 2015.

GeoSphere Austria: Geodaten zu GEOFAST - Blatt 147 Axams (1:50.000) [data set], Tethys RDR, Geologische Bundesanstalt (GBA), https://doi.org/10.24341/tethys.141, 2021

Gonzalez-Ollauri, A. and Mickovski, S. B.: Hydrological effect of vegetation against rainfall-induced landslides, J. Hydrol., 549, 374–387, https://doi.org/10.1016/j.jhydrol.2017.04.014, 2017.

https://doi.org/10.5194/egusphere-2025-2647
Preprint. Discussion started: 23 June 2025

Görüm, T.: Landslide recognition and mapping in a mixed forest environment from airborne LiDAR data, Eng. Geol., 258, 105155, https://doi.org/10.1016/j.enggeo.2019.105155, 2019.

GRASS Development Team: Geographic Resources Analysis Support System (GRASS GIS) Software, Version 8.4, Open Source Geospatial Foundation, USA, https://doi.org/10.5281/zenodo.5176030, 2024.

Greco, R., Marino, P., and Bogaard, T. A.: Recent advancements of landslide hydrology, WIREs Water, 10, e1675, https://doi.org/10.1002/wat2.1675, 2023.

Guzzetti, F.: Invited perspectives: Landslide populations – can they be predicted?, Nat. Hazards Earth Syst. Sci., 21, 1467–1471, https://doi.org/10.5194/nhess-21-1467-2021, 2021.

Guzzetti, F., Mondini, A. C., Cardinali, M., Fiorucci, F., Santangelo, M., and Chang, K.-T.: Landslide inventory maps: New tools for an old problem, Earth-Sci. Rev., 112, 42–66, https://doi.org/10.1016/j.earscirev.2012.02.001, 2012.

Jenner, A.: Ereignisdokumentation Seigesbach nach dem Hochwasserereignis in Sellrain/ Tirol am 7.6.2015, in: Tagungsband 17. Geoforum Umhausen, 17. Geoforum Umhausen, 101–110, 2015.

Koyanagi, K., Gomi, T., and Sidle, R. C.: Characteristics of landslides in forests and grasslands triggered by the 2016 Kumamoto earthquake, Earth Surf. Process. Landf., 45, 893–904, https://doi.org/10.1002/esp.4781, 2020.

Lagger, M.: Sellraintal Juni 2015: Hangexplosionen und Muren - Eine Bestandsaufnahme, in: Tagungsband 17. Geoforum Umhausen, 17. Geoforum Umhausen, 4–11, 2015.

Lague, D., Brodu, N., and Leroux, J.: Accurate 3D comparison of complex topography with terrestrial laser scanner: Application to the Rangitikei canyon (N-Z), ISPRS J. Photogramm. Remote Sens., 82, 10–26, https://doi.org/10.1016/j.isprsjprs.2013.04.009, 2013.

Land Tirol: Waldtypisierung Tirol - Waldstypen [data set], https://maps.tirol.gv.at, last access: 25 April 2025, 2014.

Land Tirol: Gewässernetz Tirol [data set], https://maps.tirol.gv.at, last access: 25 April 2025, 2023.

Li, P., Li, D., Hu, J., Fassnacht, F. E., Latifi, H., Yao, W., Gao, J., Chan, F. K. S., Dang, T., and Tang, F.: Improving the application of UAV-LiDAR for erosion monitoring through accounting for uncertainty in DEM of difference, CATENA, 234, 107534, https://doi.org/10.1016/j.catena.2023.107534, 2024.

Malamud, B. D., Turcotte, D. L., Guzzetti, F., and Reichenbach, P.: Landslide inventories and their statistical properties, Earth Surf. Process. Landf., 29, 687–711, https://doi.org/10.1002/esp.1064, 2004.

Mondini, A. C., Viero, A., Cavalli, M., Marchi, L., Herrera, G., and Guzzetti, F.: Comparison of event landslide inventories: the Pogliaschina catchment test case, Italy, Nat. Hazards Earth Syst. Sci., 14, 1749–1759, https://doi.org/10.5194/nhess-14-1749-2014, 2014.

Moser, M.: GEOFAST – Zusammenstellung ausgewählter Archivunterlagen der Geologischen Bundesanstalt 1:50.000 - 147 Axams (1:50.000), Geologische Bundesanstalt, GEOFAST 147, 2011.

ÖVDAT: Intermodales Verkehrsreferenzsystem Österreich (GIP.at) [data set], https://www.gip.gv.at, last access: 25 April 2025, 2022.

https://doi.org/10.5194/egusphere-2025-2647
Preprint. Discussion started: 23 June 2025

Pedregosa, F., Varoquaux, G., Gramfort, A., Michel, V., Thirion, B., Grisel, O., Blondel, M., Prettenhofer, P., Weiss, R., Dubourg, V., Vanderplas, J., Passos, A., Cournapeau, D., Brucher, M., Perrot, M., and Duchesnay, E.: Scikit-learn: Machine Learning in Python, J. Mach. Learn. Res., 12, 2825–2830, 2011.

Petschko, H., Bell, R., and Glade, T.: Effectiveness of visually analyzing LiDAR DTM derivatives for earth and debris slide inventory mapping for statistical susceptibility modeling, Landslides, 13, 857–872, https://doi.org/10.1007/s10346-015-0622-1, 2016.

Razak, K. A., Straatsma, M. W., van Westen, C. J., Malet, J.-P., and de Jong, S. M.: Airborne laser scanning of forested landslides characterization: Terrain model quality and visualization, Geomorphology, 126, 186–200, https://doi.org/10.1016/j.geomorph.2010.11.003, 2011.

Reichenbach, P., Rossi, M., Malamud, B. D., Mihir, M., and Guzzetti, F.: A review of statistically-based landslide susceptibility models, Earth-Sci. Rev., 180, 60–91, https://doi.org/10.1016/j.earscirev.2018.03.001, 2018.

Rickli, C. and Graf, F.: Effects of forests on shallow landslides – case studies in Switzerland, For. Snow Landsc. Res., 82, 33–44, 2009.

Roering, J. J., Schmidt, K. M., Stock, J. D., Dietrich, W. E., and Montgomery, D. R.: Shallow landsliding, root reinforcement, and the spatial distribution of trees in the Oregon Coast Range, Can. Geotech. J., 40, 237–253, https://doi.org/10.1139/t02-113, 2003.

Schaller, C., Dorren, L., Schwarz, M., Moos, C., Seijmonsbergen, A. C., and van Loon, E. E.: Predicting the thickness of shallow landslides in Switzerland using machine learning, Nat. Hazards Earth Syst. Sci., 25, 467–491, https://doi.org/10.5194/nhess-25-467-2025, 2025.

Schmaltz, E. M., Steger, S., and Glade, T.: The influence of forest cover on landslide occurrence explored with spatio-temporal information, Geomorphology, 290, 250–264, https://doi.org/10.1016/j.geomorph.2017.04.024, 2017.

Schwarz, M., Cohen, D., and Or, D.: Root-soil mechanical interactions during pullout and failure of root bundles, J. Geophys. Res. Earth Surf., 115, https://doi.org/10.1029/2009JF001603, 2010.

Taylor, F. E., Malamud, B. D., Witt, A., and Guzzetti, F.: Landslide shape, ellipticity and length-to-width ratios, Earth Surf. Process. Landf., 43, 3164–3189, https://doi.org/10.1002/esp.4479, 2018.

Virtanen, P., Gommers, R., Oliphant, T. E., Haberland, M., Reddy, T., Cournapeau, D., Burovski, E., Peterson, P., Weckesser, W., Bright, J., van der Walt, S. J., Brett, M., Wilson, J., Millman, K. J., Mayorov, N., Nelson, A. R. J., Jones, E., Kern, R., Larson, E., Carey, C. J., Polat, İ., Feng, Y., Moore, E. W., VanderPlas, J., Laxalde, D., Perktold, J., Cimrman, R., Henriksen, I., Quintero, E. A., Harris, C. R., Archibald, A. M., Ribeiro, A. H., Pedregosa, F., and van Mulbregt, P.: SciPy 1.0: fundamental algorithms for scientific computing in Python, Nat. Methods, 17, 261–272, https://doi.org/10.1038/s41592-019-0686-2, 2020.

Wehr, A. and Lohr, U.: Airborne laser scanning—an introduction and overview, ISPRS J. Photogramm. Remote Sens., 54, 68–82, https://doi.org/10.1016/S0924-2716(99)00011-8, 1999.

Zieher, T., Perzl, F., Rössel, M., Rutzinger, M., Meißl, G., Markart, G., and Geitner, C.: A multi-annual landslide inventory for the assessment of shallow landslide susceptibility – Two test cases in Vorarlberg, Austria, Geomorphology, 259, 40–54, https://doi.org/10.1016/j.geomorph.2016.02.008, 2016.